# Nickel and Palladium Complexes with New Phosphinito-Imine Ligands and Their Application as Ethylene Oligomerization Catalysts

Laura Ortiz de la Tabla, Inmaculada Matas, Pilar Palma, Eleuterio Álvarez, and Juan Cámpora*

Instituto de Investigaciones Químicas (IIQ), Consejo Superior de Investigaciones Científicas - Universidad de Sevilla, Avda. Américo Vespucio 49, 41092 Sevilla, Spain

S *Supporting Information*

ABSTRACT: Phosphinito-imines, a new class of P,N donors, are readily generated by reaction of bulky arylamide anions $[R^2CONAr]^-$ (R^2 = Me or t-Bu; Ar = 2,6-i-Pr$_2$C$_6$H$_4$) with chlorophosphines ClP(R^1)$_2$. In solution, free phosphinito-imines exist in equilibrium with the corresponding amidophosphine tautomers, containing a nitrogen-bound P(R^1)$_2$ group. However, reacting the tautomer mixtures with metal precursor complexes, such as NiBr$_2$(dme) or PdCl$_2$(cod), selectively affords stable phosphinito-imine complexes MX$_2$(P-N) (M = Ni, Pd) in excellent yields. These complexes are diamagnetic and exhibit square-planar structures in the solid state, but in solution, the Ni derivatives exchange with a small amount of the corresponding high-spin tetrahedral isomers. On treatment with MMAO or DEAC, NiX$_2$(P-N) complexes become active ethylene oligomerization catalysts, affording mainly butenes along with smaller amounts of hexenes and octenes. The activity and the selectivity of these catalysts depend on the structure of the phosphinito-imine ligand and the cocatalyst used. When activated with DEAC, complexes containing the P(i-Pr)$_2$ moiety are extremely active, achieving TOFs over 10^6 mol C$_2$H$_4$/mol Ni·h and high selectivity for butenes.
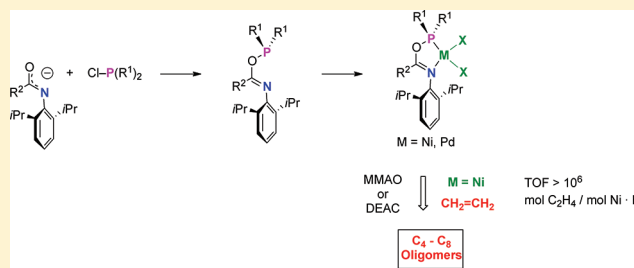
INTRODUCTION

Hybrid ligands containing hard and soft donor atoms have been widely studied and applied in organometallic chemistry and homogeneous catalysis due to the structural diversity of their complexes and their ability to impart unusual chemical reactivity.[1−5] Ligands containing P,O, P,N, or N,O donor sets introduce significant differentiation at the trans positions in the coordination sphere of a metal center, which has important consequences for the catalytic activity of such complexes.[2,6−10] Many nickel(II) complexes containing hybrid ligands have been reported to catalyze ethylene oligomerization, by favoring chain transfer over propagation during the catalytic cycle.[11−13] A reference for these are the shell higher olefin process (SHOP) catalysts. These are based on Ni complexes with anionic P,O donors and produce Schulz−Flory mixtures of oligomers with high selectivity for α-olefins.[14,15] Modification of the P,O ligands system leads to very significant changes on the catalyst selectivity[16] that can be shifted from ethylene oligomerization to polymerization, in some cases, with activities comparable to metallocene derivatives.[17] Despite the important developments achieved in this area, metal catalysts producing short-chain α-olefins with narrow Schulz−Flory distributions are still main targets.[18−20]

Nickel and palladium catalysts containing P,N ligands have received much attention in the context of ethylene oligomerization[8,10,21−35] or polymerization.[28,29,35] In general, the presence of a phosphorus donor enhances the stability of the complexes, while the imine fragment can be used for tuning the activity and selectivity of the catalyst. For instance, heterocyclic fragments, such as pyridine or oxazoline, readily incorporated in the catalyst design, have been shown to enhance the selectivity for α-olefins.[22,26] In addition, imine donor groups bearing bulky N-aryl substituents offer the possibility of a rational control of the molecular weight of the products based on the same principles established by Brookhart for α-diimine catalysts.[35−40] Such phosphino-imine complexes constitute a versatile class of catalysts giving access to products ranging from light oligomers to high-molecular-weight polymers. However, a straightforward relationship between ligand structure and catalyst activity or selectivity is not always observed, as similar ligand designs can lead to very different results.[8] One of the possible causes of such irregular behavior is the tendency of some of these ligands to undergo enolization, especially when basic cocatalysts, such as MAO, are used.[35] By using nonenolizable phosphine-imine ligands, more stable catalysts are obtained that produce higher-molecular-weight polymers.[35] The enolization problem can be avoided by replacing the H atoms on the position β to the nitrogen donor with alkyl substituents. Alternatively, this problem can be circumvented by inserting a heteroatom between the phosphorus and the imine functionality. However, direct replacement of the phosphino (R$_2$P−) for a phosphinito (R$_2$P−O−) fragment increases the chelate ring size, and this may induce changes in the geometry of the coordination sphere

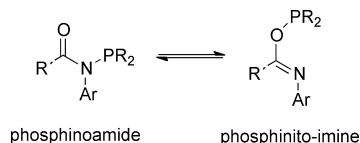around the metal center.[10,21,26,41] In contrast, phosphinito-imine ligands, depicted in Scheme 1, give rise to five-membered

Scheme 1

rings. These substances are tautomers of phosphinoamides, in which the phosphorus is bound to nitrogen. In recent years, a number of these phosphinoamide ligands have been prepared by reacting amide-based nucleophiles with chlorophosphines,[42−46] but to the best of our knowledge, neither free nor complexed phosphinito-imine tautomers have been described so far. Despite their closely related structures, the binding properties of phosphinito-imines and phosphinoamides are expected to be very different. The latter are known to coordinate solely through the phosphorus atom,[43−49] and although they can form P,O chelates,[45−47,49,50] these usually exhibit hemilabile behavior, the oxygen atom being easily displaced by incoming donor molecules.[51] However, phosphinito-imines should form strong P,N chelates. In this paper, we show that phosphinito-imine tautomers, readily prepared from carboxylic acid amides, are stabilized by steric factors when the P and N atoms bear bulky substituents. Nickel and palladium complexes of these nonenolizable P,N ligands have been prepared, and we report on their behavior as ethylene oligomerization catalysts.

■ RESULTS AND DISCUSSION

Synthesis of Ligands. The new ligands were prepared by deprotonation of N-(2,6-diisopropylphenyl)acetamide or N-(2,6-diisopropylphenyl)pivalamide with n-BuLi or NaH at −78 °C, followed by reaction with the corresponding chlorophosphines, as shown in Scheme 2. The amide anions react smoothly with chlorodiisopropylphosphine at low temperatures. In both cases, the $^{31}P\{^{1}H\}$ NMR spectra of the reaction mixtures taken after stirring for 30 min at −78 °C showed two new species in a ca. 9:1 ratio, corresponding to the tautomers **1/2** or **3/4**. Major resonances appear at ca δ 140 ppm for both the acetamide (**1**) and the pivalamide (**3**) derivatives, whereas those of secondary products are shifted upfield, at δ 90 ppm (**2**) and 65 ppm (**4**). These products show signs of thermal

instability. On standing at room temperature, the $^{31}P\{^{1}H\}$ spectra of the mixtures show that the major/minor tautomer ratio gradually decreases with simultaneous appearance of a number of signals arising from decomposition products. Products **1/2** are particularly unstable, and all attempts of isolation failed. The pivalamide derivatives **3/4** are somewhat more stable, and after extraction with diethyl ether and evaporation of the solvent, essentially pure samples containing the major isomer, **3**, were obtained, which enabled us to gather complete ^{1}H and $^{13}C\{^{1}H\}$ NMR data for this compound (see the Experimental Section).
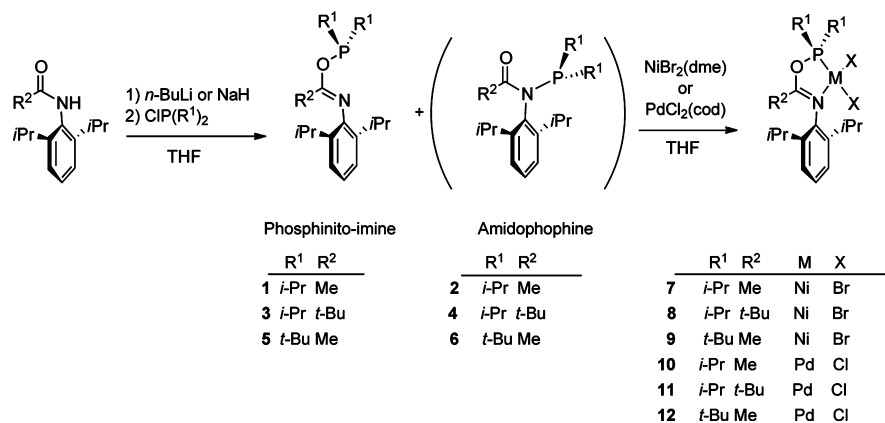
The reaction of the lithium salt of N-(2,6-diisopropylphenyl)acetamide with $ClP(t\text{-}Bu)_2$ is considerably slow, requiring 3 days at 100 °C to complete, but the products are thermally robust and do not decompose under such conditions. Again, the $^{31}P\{^{1}H\}$ NMR spectrum of the reaction mixture shows two signals at δ 142 and 65 ppm in a 95:5 intensity ratio for the corresponding tautomers (**5/6**). Crystallization from diethyl ether at −20 °C gave a small amount of a solid containing the minor component and some starting amide. Evaporation of the mother liquor afforded compound **5** as a yellow oil in 95% yield. Solutions of ligand **5** in THF are indefinitely stable at room temperature.

Although the ^{1}H and $^{13}C\{^{1}H\}$ NMR data obtained for **3** and **5** confirmed the presence of the PR_2 and the N-(2,6-diisopropylphenyl)amido groups, they provide no direct indications of whether the P atom is bound to O or N. However, the deshielding of the ^{31}P resonance of the major isomers (**1**, **3**, or **5**) suggests the presence of an electronegative O-bound group. Therefore, these can be reasonably assigned to the phosphinito-imine tautomers, whereas minor species **2**, **4**, or **6** would have the phosphinoamide structure. This hypothesis finds support in the comparison with literature $^{31}P\{^{1}H\}$ NMR phosphinites (E_2P-OR) and phosphinoamides (R_2P-NR_2). For example, the chemical shifts of the phosphinoamide-phosphinites depicted in Figure 1 are very similar to those formed in our
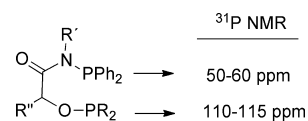
Figure 1. Typical ^{31}P chemical shifts for R_2P−N and R_2P−O linkages.

system. They give rise to low-field resonances at δ 110−150 ppm for the alkoxophosphine group and high-field ones at δ

Scheme 2

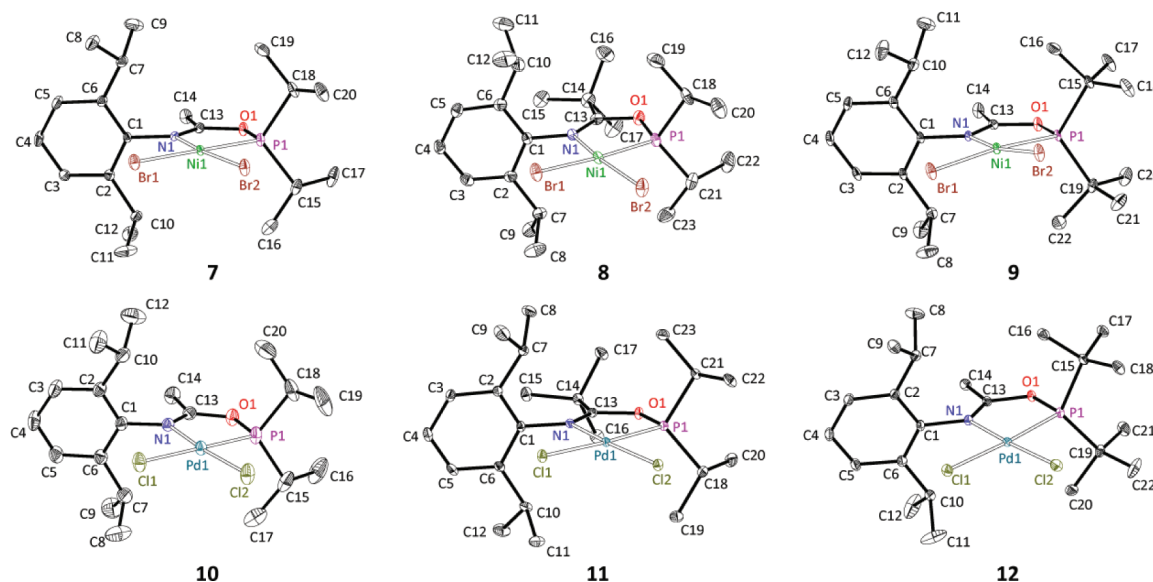|	R¹	R²			R¹	R²			R¹	R²	M	X
Phosphinito-imine				**Amidophophine**								
1	i-Pr	Me		**2**	i-Pr	Me		**7**	i-Pr	Me	Ni	Br
3	i-Pr	t-Bu		**4**	i-Pr	t-Bu		**8**	i-Pr	t-Bu	Ni	Br
5	t-Bu	Me		**6**	t-Bu	Me		**9**	t-Bu	Me	Ni	Br
								10	i-Pr	Me	Pd	Cl
								11	i-Pr	t-Bu	Pd	Cl
								12	t-Bu	Me	Pd	Cl

Figure 2. ORTEP views of complexes 7−12.

Table 1. Selected Bond Distances and Angles for Complexes 7−12 (M = Ni or Pd, X = Br or Cl)

	7	8	9	10	11	12[a]
M−P1	2.0974(9)	2.089(2)	2.1315(10)	2.1685(8)	2.1576(3)	2.2042(5)
M−N1	1.917(2)	1.955(7)	1.943(3)	2.056(2)	2.0769(10)	2.0570(12)
M−X2	2.3027(5)	2.3140(13)	2.3168(7)	2.2960(8)	2.2972(3)	2.2995(4)
M−X1	2.3318(5)	2.3371(11)	2.3477(6)	2.3552(8)	2.3748(3)	2.3637(5)
P1−O1	1.683(2)	1.675(7)	1.685(3)	1.6696(11)	1.6663(9)	1.6696(11)
O1−C13	1.341(4)	1.339(11)	1.333(5)	1.3533(17)	1.3583(14)	1.3533(17)
N1=C13	1.289(4)	1.295(9)	1.301(5)	1.282(3)	1.2916(15)	1.2873(18)
N1−C1	1.454(4)	1.440(9)	1.449(5)	1.456(3)	1.4454(15)	1.4533(18)
X2−M−X1	94.710(18)	93.28(5)	92.46(2)	93.98(3)	93.545(12)	90.735(14)
X1−M−N1	97.02(8)	99.41(17)	96.36(10)	95.66(6)	97.54(3)	94.56(3)
X2−M−P1	83.81(3)	83.43(7)	87.32(3)	88.38(3)	87.077(12)	92.866(15)
X2−M−N1	168.06(8)	166.34(17)	169.54(10)	170.17(6)	168.34(3)	174.60(3)
X1−M−P1	178.50(3)	173.14(9)	173.73(4)	177.33(3)	177.284(12)	176.155(13)
P1−M−N1	84.47(8)	84.47(18)	84.53(10)	81.94(6)	82.02(3)	81.87(3)
M−N1−C1	123.36(2)	118.7(4)	125.3(2)	123.28(2)	116.41(7)	123.04(9)
C13−N1−C1	116.4(2)	122.0(7)	115.6(3)	117.9(2)	124.3(1)	117.9(1)
X1−X2−P1−N1	2.14	8.24	8.84	2.14	4.81	1.85[b]

[a]One of two independent molecules. [b]7.08° in molecule 2.

50−60 ppm for the phosphinoamide.[52] It seems very likely that the relative stability of the phosphinito-imine and phosphinoamide tautomers is determined by steric factors. The phosphinoamide tautomer, usually favored over the phosphinito-imine,[42−46] becomes destabilized in our system by the steric repulsions posed by the bulky PR$_2$ and N-Ar groups.

Nickel and Palladium Phosphinito-Imine Complexes. Reacting freshly prepared mixtures of tautomers (1/2 or 3/4) or the purified ligand 5 with equimolar amounts of NiBr$_2$(dme) (dme = 1,2-dimethoxyethane) or PdCl$_2$(cod) (cod = 1,5-cyclooctadiene) leads exclusively to the Ni(II) and Pd(II) complexes 7−12 containing the P,N phosphinito-imine ligands (Scheme 2). The ^{31}P{^{1}H} spectra of crude reaction mixtures display a single resonance, confirming that only one isomer is produced. Thus, a rapid isomerization of the minor phosphinoamide tautomer takes place on complexation to the metal center. After workup, the complexes were isolated as crystalline, diamagnetic solids. In contrast with the free ligands, their complexes are thermally stable and can be exposed to air

for short periods of time without noticeable decomposition. The diamagnetism of the nickel derivatives indicates that the phosphinito-imine ligand favors square-planar structures both in the solid state and in solution. This is somewhat unusual, for most P,N ligands form paramagnetic complexes with NiX$_2$ moieties.[21−37]

The P,N coordination mode is supported by the ^{31}P{^{1}H} and IR data and confirmed by the X-ray structures of the complexes. The phosphorus spectra show low-field resonances at ca. 200 ppm for the palladium derivatives and 166−198 ppm for their nickel analogues, which is more consistent with an R$_2$P-O than with an R$_2$P-N fragment. In addition, ν(C=N) absorption bands are observed in the 1590−1650 cm^{-1} region of the infrared spectra. The imine absorption of free ligand 5 at 1679 cm^{-1} shifts by ca. 20 cm^{-1} to lower frequency upon coordination to Ni and Pd in complexes 9 and 12.

All complexes 7−12 have been characterized by X-ray diffraction. Their crystal structures are shown in Figure 2, and main bond distances and angles are collected in Table 1. All
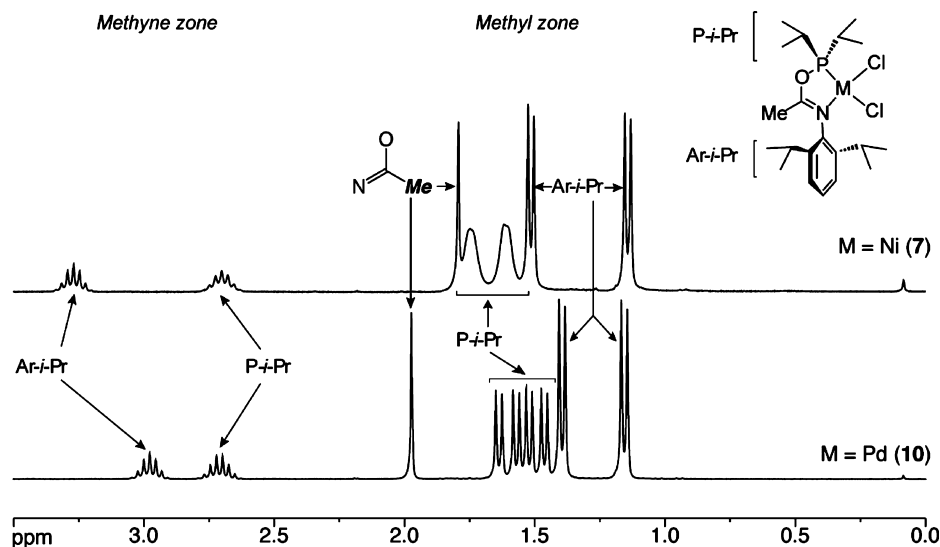
Figure 3. Room-temperature spectra of complexes **7** and **10** (CD$_2$Cl$_2$ high-field region only).

molecules are characterized by the flat five-membered N,P chelate and a square-planar coordination environment, with very small tetrahedral distortion. The distortion degree is measured by the torsion angle formed by the halide ligands and the P and N atoms (X1X2P1N1). This is very small and virtually identical for both complexes of ligand **1**, but the derivatives of the relatively bulky ligands **3** and **5** show a slight tetrahedral distortion, somewhat larger for the Ni (ca. 8°) than for the Pd complexes. The intra-annular P–O, O–C, and C=N distances are unexceptional and essentially identical in all the complexes. The aryl ring lies perpendicular to the coordination plane, leaving the isopropyl groups pointing toward the axial positions of the metal center. In the pivalamide derivatives **8** and **11**, the aryl ring is forced by the steric pressure of the bulky *t*-Bu substituent to come closer to the metal fragment. This is reflected in the wider C13–N1–C1 and narrower C1–N1–M angles in these complexes. The lengths of M–X bonds sense the different trans influence of the P and N donors, and those opposed to the more strongly donor phosphinito group are appreciably longer than those trans to the imine fragment. Although the lengths of Ni–Br and Pd–Cl are similar, the differential effect of trans groups is less pronounced for Ni complexes (ca. 1.2% of the average length) than in the Pd derivatives (2–3%). Complex **11** exhibits the largest d_{M-X1}–d_{M-X2} difference, due to the extra elongation of the Pd–Cl1. This is probably caused by the steric pressure originated by the *t*-Bu substituent of the phosphinito-imine backbone, transmitted by the aryl ring to the nearby chloride ligand. The pressure of the aryl ring on the Ni–Br1 bond of **8** has no noticeable effect on its length because it is efficiently released by the significant tetrahedral distortion of this complex.

As discussed above, the diamagnetic, square-planar configuration of the Ni complexes is unusual among (P-N)NiX$_2$ complexes. Some examples of square-planar Ni(II) derivatives of phosphinito-pyridine ligands have been reported, which display square-planar structures in the solid state,[23,26] but are paramagnetic in solution.[23] The NMR spectra of the phosphinito-imine complexes of Ni and Pd in CD$_2$Cl$_2$ are very similar and typical of diamagnetic compounds, showing that their square-planar configurations are retained in solution. However, the room-temperature spectra of the Ni complexes reveal some intriguing differences with those of their Pd

counterparts. The spectra of the latter show sharp and well-defined signals, whereas the ^{31}P signals of the Ni complexes are broad and H–P couplings in the ^{1}H spectrum appear partially unresolved. Notably, signals arising from the P-bound isopropyl groups of the Ni complex appear broadened, whereas those of the 2,6-substituents of the aryl group are sharp and well-resolved. These differences can be clearly seen in the high field region of the ^{1}H spectra of compounds **7** and **10**, represented in Figure 3, and suggest the occurrence of some fluxional process. To ascertain its nature, variable-temperature ^{1}H and ^{31}P NMR studies were carried out on complex **7** and its Pd analogue, **10**. The spectrum of the latter is essentially temperature-independent within the studied temperature range, but those of the nickel compound display significant shape variations. Below 253 K, the slow exchange limit is reached and the spectrum shows well-resolved H–P couplings. As the temperature rises, couplings to phosphorus progressively fade away in the proton spectra while the ^{31}P signal becomes broader. At 323 K, the latter disappears in the baseline, and H–P couplings are totally lost in the ^{1}H spectrum.

Selective loss of couplings is a common phenomenon in the NMR spectra of coordination or organometallic complexes. This phenomenon normally stems from the reversible dissociation of the bonds responsible for the transmission of the coupling. Obviously, this is not the case here since reversible P–C bond dissociation cannot occur. A rapid exchange between the diamagnetic square-planar complex with small amounts of a high-spin ($S = 1$) tetrahedral isomer might account for the observations and is in good agreement with the absence of similar effects in the spectra of the Pd derivatives (Figure 4). Because the ^{31}P atom is directly bound to the metal center, hyperfine coupling to the electronic spin provides an extremely efficient relaxation mechanism, leading to the observed broadening of the P resonance and to the effective cancellation of heteronuclear couplings to phosphorus. Assuming this explanation, a simulation of the methyl region of the ^{1}H spectrum line shape has been carried out (Figure 5; see the Experimental Section for details). Figure 6 shows the Eyring plot for the computed exchange rates, which provide the following activation parameters for the exchange process: $\Delta H^{\ddagger}$ = 10.4(9) kcal/mol, $\Delta S^{\ddagger}$ = −4(1) cal/mol·K, and $\Delta G^{\ddagger}$ = 11.66(15) kcal/mol at 298 K. According to Hammond's
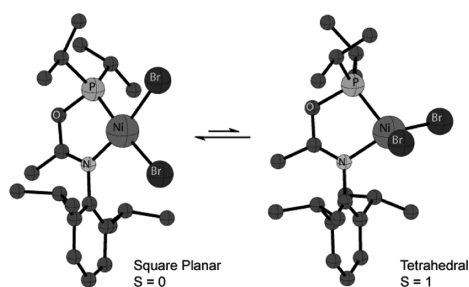
Figure 4. Square-planar and tetrahedral geometries for complex **7** (BP86-optimized structures).
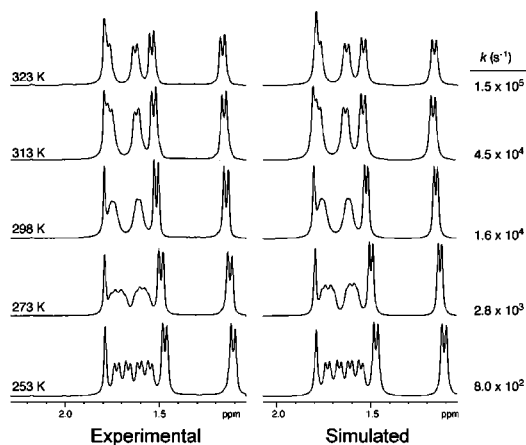

Figure 5. Experimental and simulated ^{1}H NMR spectra of compound **7** recorded at variable temperatures (methyl zone).
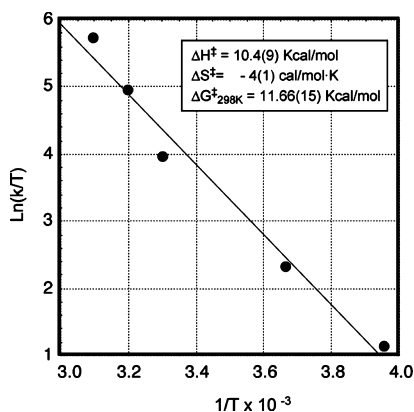

Figure 6. Eyring plot (253−323 K) of the computed rate constants and activation parameters.

postulate, the energy of the tetrahedral form probably is only slightly lower than the barrier of the observed exchange process. To assess this hypothesis, DFT calculations were performed to determine the relative energies of the square-planar and tetrahedral forms. As a first option, the hybrid functional B3LYP was used, but the calculation incorrectly predicted that the tetrahedral isomer should be more stable than the square-planar by 3.0 kcal/mol. However, a second calculation with the pure functional BP86 provides the correct energy order with the tetrahedral species lying 10.6 kcal/mol above the diamagnetic ground state, in good agreement with the experiment. It is known that, at least for some types of transition-metal complexes, pure gradient-corrected functionals, such as BP86, perform better for the purpose of estimating spin

state splitting energies.[53] The structures representing the square-planar and tetrahedral forms of **7** shown in Figure 4 correspond to the BP86-optimized geometries.

Catalytic Behavior of Phosphinito-Imine Complexes. Catalytic Oligomerization of Ethylene. The catalytic activity of complexes **7−12** was investigated using modified methylalumoxane (MMAO) or diethylaluminum chloride (DEAC) as cocatalysts in toluene as a solvent. The reactions were performed in 250 mL Fischer-Porter glass reactors fitted with an internal thermocouple and a septum-capped port for catalyst injection. The reactors were immersed in a thermostatic water bath at a preset temperature. Ethylene consumption and the internal reactor temperature were monitored continuously during the experiments.

The catalysts were screened in a series of experiments at 30 °C and an ethylene pressure of 5 bar (standard conditions), which showed that the Ni complexes actively catalyze the oligomerization of ethylene into mixtures of butenes, hexenes, and octenes, whereas the Pd complexes are catalytically inactive. No polyethylene precipitates when the reaction mixtures are treated with acidified methanol. In general, the results of quantitative GC analysis are in good agreement with the ethylene consumption data, confirming that no high-molecular-weight oligomers or polymers are produced. The Ni catalysts display low thermal stability, since their activity is sensibly reduced at 50 °C and becomes negligible at 70 °C.

The preliminary study was extended to determine the optimum [Ni]/[Al] ratios (Table 2). Complex **7** achieves its

Table 2. Influence of the Catalyst/Cocatalyst Ratio on the Activity of Complexes 7−9[a]

catalyst	co-catalyst	[Al]/[Ni]	TOF × 10^{-3}	catalyst	co-catalyst	[Al]/[Ni]	TOF × 10^{-3}
7	MMAO	1000	10.4	7[b]	DEAC	250	186.9
7	MMAO	750	14.9	7[b]	DEAC	200	389.7
7	MMAO	500	17.5	7[b]	DEAC	175	834.4
7	MMAO	250	20.1	7[b]	DEAC	150	866.2
7	MMAO	150	12.8	7[b]	DEAC	100	528.3
8	MMAO	1000	7.4	7[b]	DEAC	50	518.1
8	MMAO	500	9.8	8	DEAC	175	22.9
9	MMAO	700	2.2	9	DEAC	300	54.6
9	MMAO	600	2.6	9	DEAC	200	36.9
9	MMAO	500	2.2	9	DEAC	100	20.2
9	MMAO	400	1.8	9	DEAC	50	14.0
9	MMAO	200	1.9				

[a]Experimental conditions: [Ni] = 2 × 10^{-4} M; solvent, toluene; total volume ≈ 20 mL; 30 °C; 4 bar. Reaction time, 1 h, unless otherwise stated. [b]Reaction time 3−5 min.

best performance with relatively low loads of either MMAO or DEAC (200 or 150 equiv, respectively). Although **8** and **9** can also be activated with similar amounts of DEAC (**8**: 150 equiv; **9**: 200 equiv), with MMAO, a higher [Al]/[Ni] ratio of ca. 600 is required for efficient performance. In general, the effect of the catalyst/cocatalyst ratio on the activities is not dramatic, but DEAC behaves as a much more effective cocatalyst than MMAO.

Tables 3 and 4 collect data for a set of 60 min experiments carried out to compare the effect of catalyst structure, pressure, and temperature on the catalytic activity and selectivity of the three nickel complexes. Complexes **7** and **8** exhibit very similar catalytic properties and are much more active than **9**. Upon

Table 3. Activity and Selectivity Data for Ethylene Oligomerization with Complexes 7−9 Activated with MMAO[a]

	cat	$[Ni]^b \times 10^{-5}$	$[Al]^b \times 10^{-2}$	P^c (bar)	T^d (°C)	$yield^e$ (grs)	$TOF^f \times 10^{-3}$ (h^{-1})	max $TOF^g \times 10^{-3}$ (h^{-1})	$TOF_{60}^h \times 10^{-3}$ (h^{-1})	$t_{1/2}^i$ (min)	ΔT^j (°C)	$C_4{:}C_6{:}C_8$	$C_4{:}1{-}C_4H_8/2{-}$ trans/2-cis
1	7	21.0	4.4	5	30	3.41	13.5	37.8	4.0	12	4.7	78:20:3	13:30:57
2	7	2.6	4.1	5	30	0.33	8.9	15.9	8.0	60	0.2	71:29:0	29:11:60
3	7	2.6	4.1	9	30	0.52	16.6	25.0	12.4	>60	2.1	71:29:0	41:9:50
4	7	21.0	4.4	5	0	3.76	14.8	37.1	10.0	13	5.0	83:12:5	8:25:67
5	8	20.1	12.1	5	30	1.39	16.4	71.1	6.0	8	9.9	64:23:13	27:16:58
6	8	2.6	12.5	5	30	0.16	5.2	28.9	2.1	7	0.3	77:23:0	61:11:28
7	8	10.3	12.3	9	30	4.62	36.6	102.3	23.6	11	7.3	77:20:3	16:14:70
8	8	20.0	12.0	5	0	2.77	11.0	36.7	6.9	9	5.3	80:17:3	19:23:58
9	8	10.2	12.0	5	0	1.10	14.7	36.8	55.3^k	>60	1.9	81:17:2	29:20:51
10	9	20.0	12.0	5	30	0.10	0.4	2.2	0.0	8	1.4	50:40:10	100:0:0
11	9	20.0	12.0	5	30	0.23	0.9	7.7	0.0	7	1.7	54:42:4	94:3:4
12	9	20.0	12.0	9	30	0.09	0.4	9.0	0.0	7	0.5	66:34:0	94:3:4
13	9	20.0	12.0	5	0	2.18	8.6	26.8	2.8	14	6.3	65:31:4	94:2:3

[a]Reaction time, 60 min; total volume, 42 mL; solvent, toluene. [b]mol·L^{−1}. [c]Ethylene pressure. [d]External bath temperature. [e]Oligomer yield, from GC analysis. [f]Average activity (TOF, in mol ethylene/mol Ni·h). [g]Maximum TOF, from ethylene consumption curves. [h]Activity after 60 min. [i]Time for 50% activity decay. [j]Increase of internal reactor temperature. [k]Reaction rate increases continuously during the experiment.

Table 4. Activity and Selectivity Data for Ethylene Oligomerization with Complexes 7−9 Activated with DEAC[a]

	cat	$[Ni]^b \times 10^{-5}$	$[Al]^b \times 10^{-2}$	P^c (bar)	T^d (°C)	$yield^e$ (grs)	$TOF^f \times 10^{-3}$ (h^{-1})	max $TOF^g \times 10^{-3}$ (h^{-1})	$TOF_{60}^h \times 10^{-3}$ (h^{-1})	$t_{1/2}^i$ (min)	ΔT^j (°C)	$C_4{:}C_6{:}C_8$	$C_4{:}1{-}C_4H_8/2{-}$ trans/2-cis
1	7	2.6	3.1	5	30	2.43	77.5	1662.5	0.0	5	27.0	80:20:0	48:31:21
2	7	1.0	3.1	5	30	1.94	154.1	738.0	0.0	6	5.9	88:12:0	40:23:37
3	7	1.0	3.1	9	30	3.13	240.2	3837.6	0.0	9	25.3	87:12:0	50:20:30
4	7	2.6	3.1	5	0	0.31	9.9	12.5	12.5^k	>60	0.9	88:12:0	17:34:49
5	8	19.9	3.5	5	30	18.57	73.5	322.9	5.0	22	40.6	75:23:0	17:46:37
6	8	2.6	3.1	5	30	3.05	96.8	1812.6	0.0	4	30.1	82:18:0	32:30:18
7	8	2.6	3.1	9	30	4.26	135.3	1685.3	5.2	4	45.2	84:14:1	36:31:33
8	8	10.3	3.1	5	0	12.57	99.7	490.3	0.0	9	54.8	81:18:2	4:51:45
9	9	19.7	3.9	5	30	2.63	10.4	13.8	7.0	60	1.2	90:10:0	33:41:25
10	9	19.7	3.9	9	30	3.69	14.7	17.5	14.6	41	0.9	98:2:0	0:77:23
11	9	19.7	3.9	5	0	0.81	2.2	6.8	1.4^k	>60	5.3	93:14:0	42:25:33

[a]Reaction time, 60 min; total volume, 42 mL; solvent, toluene. [b]mol·L^{−1}. [c]Ethylene pressure. [d]External bath temperature. [e]Oligomer yield, from GC analysis. [f]Average activity (TOF, in mol ethylene/mol Ni·h). [g]Maximum TOF, from ethylene consumption curves. [h]Activity after 60 min. [i]Time for 50% activity decay. [j]Increase of internal reactor temperature. [k]Reaction rate increases continuously during the experiment.
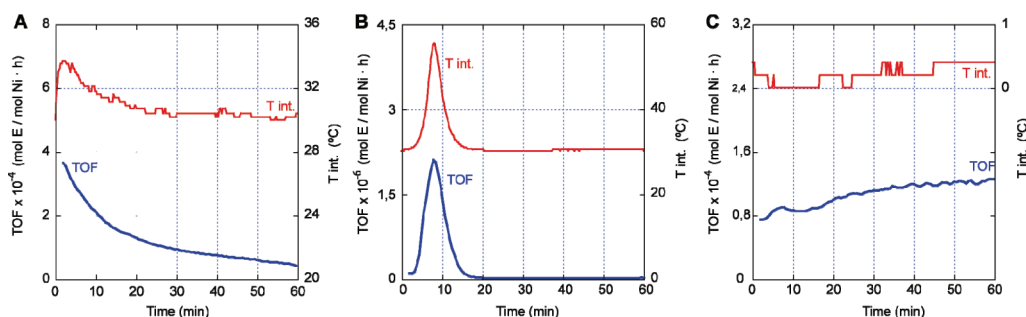

Figure 7. Representative examples of activity profiles observed with phosphinito-imine catalysts. The lower curve (blue) represents the activity variation (TOF) and the upper (red), the internal reactor temperature. (A) Typical activity curve, corresponding to entry 1, Table 3. (B) "Pulsed" activity, showing a narrow activity maximum, entry 3, Table 4. (C) Slow catalyst activation at low temperature, entry 4, Table 4.

activation with DEAC or MMAO, **7** and **8** give rise to very active catalysts, achieving ethylene turnover frequencies well above 10^6 mol ethylene/mol Ni·h^{−1} under favorable conditions. Monitoring ethylene consumption shows that, upon activation at 30 °C, the activity reaches its peak within a few seconds or minutes, decaying afterward during the rest of the experiment (Figure 7A). The activation process is accompanied by a visible color change of the mixture from the characteristic purple-red of the complexes to yellow. However, as discussed below, the

use of diluted catalyst solutions or lower operating temperatures may lead to very different activity profiles. Apart from the typical example A, Figure 7 shows other two significant examples of such profiles, B and C.

Although catalysts produced with DEAC are more active than those generated with MMAO, the latter are longer lived. For example, the time required by the catalytic activity to fall to 50% of its maximum value ($t_{1/2}$) is 4−6 min with **7** or **8** when activated with DEAC and >7 min with MMAO under standard

conditions. In contrast, the catalyst formed with **9** and DEAC shows low, but sustained, activity under the same conditions (Table 4, entry 9). A possible explanation for the faster deactivation of **7**–**8**/DEAC is that heat released by the high activity levels favors catalyst decomposition. As can be seen in Figure 7, the internal reactor temperature parallels the activity profile, temperature peaks of 30−40 °C being observed when high activity levels are reached. In most cases (profile A), after the initial activity peak, the temperature declines and the catalyst performance reaches an almost stable regime in which the activity decay is relatively slow. With MMAO, the catalysts retain significant activity after 60 min runs (TOF_{60}), whereas DEAC-activated systems are usually inactive before the end of the experiments. To avoid excessive heating, the dose of the nickel catalyst was decreased according to the activity observed in preliminary experiments, while maintaining other parameters, such as the cocatalyst concentration and reaction volume, constant. However, even under high dilution conditions, systems generated from **7** or **8** and DEAC are active enough to induce significant temperature peaks (entries 2, 3, 6, and 7, Table 4). After the sharp activity maximum, the catalyst deactivates, resulting in a fast reaction "pulse" rather than a sustained process (profile B). In an attempt to increase the rate of heat transfer, we used external cooling to 0 °C, but at this temperature, catalyst performance becomes limited by incomplete activation (profile C). In these experiments (Table 3, entries 4 and 9, and Table 4, entry 9), ethylene consumption curves show that the activity rises slowly, in some cases, without even reaching a true maximum. In experiment 8, Table 4, the 0 °C bath was used in combination with a larger load of catalyst **8**. This induced faster catalyst activation, but the internal temperature rose to nearly the same level observed under standard conditions, resulting in a similar deactivation rate.

The influence of the ethylene pressure on the activity of complexes **7**–**9** is not clear-cut. In general, the average activity increases by a factor of 1.5−2 when the pressure rises from 5 to 9 bar (compare, for example, entries 2 and 3 in Table 3, or entries 6 and 7 in Table 4). The origin of this effect is not evident, because global productivity figures do not depend exclusively on the specific activity of the catalyst but also on its decay rate, which can be, in turn, influenced by monomer concentration, as well as by changes in the internal reactor temperature. Complex relationships between these factors lead to the different activity profiles, such as those illustrated by Figure 7, which makes it very difficult to extract any conclusion from the mere comparison of average experiment activity. In part, the positive influence of pressure on global productivity might originate in a decrease of the catalyst decay rate. Indeed, catalysts survive somewhat longer in experiments carried out at 9 bar than at 5 bar, as evidenced by increases in $t_{1/2}$ or TOF_{60}. Because catalyst deactivation probably has only a minor effect on the maximum activity level that the catalysts achieve shortly after the beginning of the experiment (TOF_{max}), this is a better descriptor for the effect of pressure on the specific catalyst activity. However, for very active systems, TOF_{max} could be biased by mass transport effects and by the simultaneous increase of the internal temperature. Thus, experiments developing mild activities are probably best suited for the analysis of the pressure effect. Thus, for complexes **7** and **8** activated with MMAO, the TOF_{max} parameter increases significantly on going from 5 to 9 bar, suggesting that the rate-limiting step is directly dependent on the monomer concentration. However, the less-active catalyst **9** is insensitive

to pressure changes (with either MMAO or DEAC). This difference suggests that the rate-determining step of the ethylene oligomerization process could be different for the latter.

The C4/C6/C8 selectivity ratio of the Ni phosphino-imine catalysts is hardly influenced by temperature or pressure, but there is a dramatic effect of the nature of the cocatalyst. Activation with DEAC increases the selectivity for C4 products and leads to lower amounts of hexenes and octenes than MMAO. Diagrams shown in Figure 8 represent the average
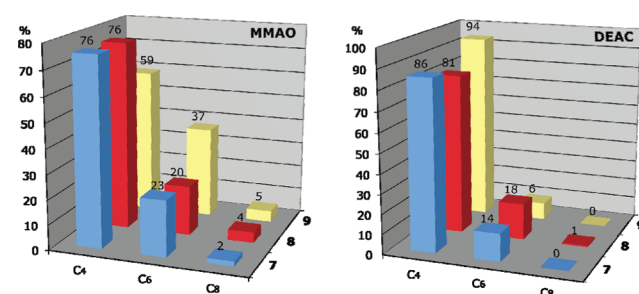

Figure 8. Selectivity of complexes **7**–**9** for ethylene oligomerization upon activation with MMAO and DEAC, calculated as averages for all experiments. Percent values (%) are given on the top of each column.

product distributions obtained for each of these catalyst/cocatalyst combinations in the studied ranges of pressure and temperature. As can be seen, complexes **7** and **8** bear a remarkable resemblance in terms of selectivity, whereas the profile of the mixtures of oligomers generated with **9** is less alike. Curiously, whereas the latter forms the least-selective catalyst when activated with MMAO, with DEAC, it produces almost exclusively butenes with >90% selectivity.

The ratio of 1-butene and 2-cis- and 2-trans-butene is widely variable, probably due to secondary isomerization reactions that are difficult to control. Complex **9** is again exceptional on this regard, since, in combination with MMAO, the C4 fraction produced consistently contains >94% 1-butene, suggesting that the isomerization process does not operate in this case. This selectivity is not seen with DEAC.

The preference of the nickel phosphinito-imine catalysts for ethylene dimerization is rather surprising considering that these compounds contain a 2,6-diisopropylphenylimino group, which is specifically designed to increase the molecular weight of the products by hindering chain transfer to the monomer.[54−58] Indeed, structurally related phosphino-imine complexes containing the same bulky aryl substituent produce either heavy Schulz−Flory mixtures of oligomers[37] (with α = 0.8−0.9) or medium- to high-molecular-weight polyethylenes.[27,29] The similarity of the product distributions obtained with **7** and **8** and the differences observed for **9** suggest that selectivity is controlled by the PR^1_2 group, while it is relatively insensitive to changes in the α substituent of the imine fragment (Me or *t*-Bu). The different behavior of phosphinito-imine and phosphine-imine complexes and the lack of significant effects of substituents on the ligand backbone could be taken as an indication of significant alterations of the phosphinito-imine ligand on activation by aluminum cocatalysts, that is, cleavage of the P−O bond leading to imine-free species. However, the oligomer distribution is reminiscent of those obtained with Ni catalysts containing phosphinito-heterocycle[10,26] and other P,N ligands.[23,25] Furthermore, Braunstein has shown that phosphi-

nito-type ligands form stable complexes with aluminum alkyls without P−O cleavage.[26] If the phosphinito-imine chelates maintain their integrity under our catalysis conditions, an unusually low energy barrier for the chain transfer process would be necessary to explain the selectivity for low-molecular-weight products.

CONCLUSIONS

A new family of phosphinito-imine ligands is readily available from the reaction of the anions of the bulky amides N-(2,6-diisopropylphenyl)acetamide or N-(2,6-diisopropylphenyl)-pivalamide with chlorodiisopropylphosphine or chlorodi-*tert*-butylphosphine. The new ligands are formed together with minor amounts of the corresponding amidophosphine tautomers. However, upon reaction with suitable precursors, such as NiBr₂(dme) or PdCl₂(cod), the mixtures are cleanly transformed into the phosphinito-imine complexes **7**−**12**, which are obtained in excellent yields and are thermally stable in solution and in the solid state. These have square-planar structures characteristic of a low-spin configuration, although in solution, the nickel complexes undergo exchange with the high-spin tetrahedral isomer with $\Delta G^{\ddagger} = 11.66(15)$ kcal/mol. Upon activation with MMAO or DEAC, nickel complexes **7**−**9** become active ethylene oligomerization/polymerization catalysts, producing mainly butenes, and minor amounts of hexenes and octenes. Both the activity and the selectivity of these catalysts are strongly influenced by the nature of the cocatalyst. In general, DEAC leads to higher activities and better selectivities for ethylene dimerization. Complexes **7** and **8** have very similar catalytic properties, reaching extremely high catalytic activities (TOF), over 10^6 h^{-1} when activated with DEAC. Catalysts generated from **9** are considerably less active but offer somewhat improved selectivity control, allowing >90% butenes when activated with DEAC, and high selectivity for α-olefins with MMAO.

EXPERIMENTAL SECTION

General Considerations. All experiments were carried out under dry nitrogen using standard Schlenk techniques. Solvents were rigorously dried and degassed before use. Microanalyses were performed by the Microanalytical Service of the Instituto de Investigaciones Químicas (Sevilla, Spain). Infrared spectra were recorded on a Bruker Vector 22 spectrometer, and NMR spectra on Bruker DRX 400 and 500 MHz and Bruker DPX 300 MHz spectrometers. The ^{1}H and ^{13}C{^{1}H} NMR resonances of the solvent were used as the internal standard, but the chemical shifts are reported with respect to TMS. ^{31}P NMR resonances are referenced to external 85% H₃PO₄. NMR chemical shifts are given in parts per million and coupling constants in hertz. GC analyses were performed in an Agilent model HP 6890 chromatograph equipped with a HPGASPRO column and a TCD detector, using CH₂Cl₂ as the internal standard. Compounds NiBr₂(dme)[59] and PdCl₂(cod)[60] were prepared according to literature procedures. The amides 2,6-iPr₂C₆H₃NHC-(O)Me and 2,6-iPr₂C₆H₃NHC(O)-t-Bu were synthesized by standard procedures.[61]

Ligand 1. A solution of the amide 2,6-iPr₂C₆H₃NHC(O)Me (219 mg, 1 mmol) in THF (20 mL), stirred at −78 °C, was successively treated with 0.63 mL (1 mmol) of a 1.6 M solution of nBuLi in hexane, and 0.167 mL (1 mmol) of iPr₂PCl. The stirring was continued for 30 min at the same temperature, and the solution was directly used for the synthesis of the complexes. This solution contains a mixture of the corresponding phosphinito-imine (**1**) and phosphinoamide (**2**) tautomers. ^{31}P{^{1}H} NMR (25 °C, THF, 121 MHz): two signals in a ca. 90:10 intensity ratio at δ 139.0 (s, isomer **1**) and 90.0 (s, isomer **2**).

Ligand 3. Sodium hydride (14 mg, 0.6 mmol) was suspended in a solution of the amide 2,6-iPr₂C₆H₃NHC(O)tBu (150 mg, 0.57 mmol) in 10 mL of THF. The mixture was stirred at 40 °C for 1 h. After removing the NaH excess by centrifugation, the solution was cooled to −78 °C, and 0.5 mL of a 1 M solution of iPr₂PCl (0.5 mmol) in THF was added with stirring. The mixture was allowed to react at the same temperature for 30 min. The resulting solution, containing a ca. 90:10 mixture of the phosphinito-imine (**3**) and phosphinoamide (**4**) tautomers, was used directly for the synthesis of the complexes. ^{31}P{^{1}H} NMR (25 °C, THF): δ 140.2 (s, isomer **3**), 65.0 (s, isomer **4**). A spectroscopically pure sample of **3** was obtained by evaporating the solvent under reduced pressure, extracting the residue with diethyl ether, filtering, and taking the solution to dryness. ^{1}H NMR (25 °C, CD₂Cl₂, 300 MHz): δ 1.07 (dd, 6H, $^3J_{HH}$ = 7 Hz, $^3J_{HP}$ = 14 Hz, PCH*Me*Me), 1.16 (dd, 6H, $^3J_{HH}$ = 7 Hz, $^3J_{HP}$ = 11 Hz, PCHMe*Me*), 1.24 (s, 9H, tBuC(O)N), 1.33 (d, overlapping signal, aryl-CH*Me*Me), 1.35 (d, overlapping signal, aryl-CHMe*Me*), 1.83 (m, 2H, PCHMe₂), 3.09 (hept, 2H, $^3J_{HH}$ = 7 Hz, aryl-CHMe₂), 7.08 (t, 1H, $^3J_{HH}$ = 7 Hz, p-CH$_{ar}$), 7.14 (d, 2H, $^3J_{HH}$ = 7 Hz, m-CH$_{ar}$). ^{13}C{^{1}H} NMR (25 °C, CD₂Cl₂, 75 MHz): δ 17.8 (d, $^2J_{CP}$ = 3 Hz, PCH*Me*Me), 17.9 (s, PCHMe*Me*), 22.6 (s, aryl-CH*Me*Me), 23.9 (s, aryl-CHMe*Me*), 27.9 (d, $^1J_{CP}$ = 23 Hz, PCHMe₂), 28.8 (s, *Me*₃CC(O)N), 29.1 (s, aryl-CHMe₂), 30.4 (s, Me₃CC(O)N), 122.6 (s, m-CH$_{ar}$), 123.2 (s, p-CH$_{ar}$), 136.4 (s, N-C$_{ar}$), 143.2 (s, o-C$_{ar}$), 160.7 (d, $^2J_{CP}$ = 6 Hz, Me₃CC(O)N).

Ligand 5. A glass ampule with a Young Teflon tap and magnetic stirrer was charged with a THF solution of 2,6-iPr₂C₆H₃NHC(O)Me (1.2 g, 5.86 mol) in 20 mL of THF. The solution was cooled to −78 °C and treated with 3.66 mL of a 1.6 M solution of nBuLi in hexane (5.86 mmol). After stirring for 5 min at this temperature, 1.017 g (5.86 mmol) of tBu₂PCl was added. The cooling bath was removed, the tap was closed, and the mixture was stirred at 100 °C for 3 days. The resulting solution contains a 95:5 mixture of **5** and **6**. ^{31}P{^{1}H} NMR (25 °C, THF, 121 MHz): δ 142.3 (s, **5**), δ 65.4 (s, **6**). The solvent was then removed under reduced pressure, and the residue was extracted with 50 mL of CH₂Cl₂. The solution was evaporated again, and the residue was dissolved in diethyl ether. A white solid containing the phosphinoamide tautomer **6** and some starting amide precipitated when the solution was stored at −30 °C. The solution was filtered and taken to dryness, leaving **5** as a yellow oil. Yield: 95% (2.02 g). IR (THF solution): v(C═N) 1679 cm^{-1}. ^{1}H NMR (25 °C, C₆D₆, 300 MHz): δ 1.11 (d, 6H, $^3J_{HH}$ = 7 Hz, aryl-CH*Me*Me), 1.14 (d, 6H, $^3J_{HH}$ = 7 Hz, aryl-CHMe*Me*), 1.21 (d, 18H, $^3J_{HP}$ = 12 Hz, P(t-Bu)₂), 1.76 (s, 3H, *Me*C(O)N), 2.87 (hept, 2H, $^3J_{HH}$ = 7 Hz, aryl-CHMe₂), 7.02 (t, 1H, $^3J_{HH}$ = 7 Hz, p-CH$_{ar}$), 7.1 (d, 2H, $^3J_{HH}$ = 7 Hz, m-CH$_{ar}$). ^{13}C{^{1}H} NMR (25 °C, C₆D₆, 75 MHz): δ 17.7 (s, *Me*C(O)N), 23.1 (s, aryl-CH*Me*Me), 23.5 (s, aryl-CHMe*Me*), 27.6 (d, $^2J_{CP}$ = 17 Hz, PC*Me*₃), 28.3 (s, aryl-CHMeMe), 35.1 (d, $^1J_{CP}$ = 28 Hz, PCMe₃), 123.1 (s, m-CH$_{ar}$), 123.3 (s, p-CH$_{ar}$), 138.1 (s, o-C$_{ar}$), 144.3 (s, N-C$_{ar}$), 160.7 (d, $^2J_{CP}$ = 6 Hz, MeC(O)N).

Synthesis of Ni[N-(2,6-iPr₂C₆H₃)═C((CH₃)OPiPr₂)]Br₂ (7). A THF solution of ligand **1** (1 mmol) prepared in situ as described above was added to a suspension of NiBr₂(dme) (308 mg, 1 mmol) in 10 mL of THF cooled to −40 °C. The reaction mixture was allowed to warm to room temperature. After stirring for 30 min, the solvent was evaporated under vacuum, and the red residue was extracted with 60 mL of CH₂Cl₂ and filtered. The solution was then taken to dryness, and the residue was washed with 2 × 20 mL of hexane and recrystallized from a mixture CH₂Cl₂/toluene (2:1) at −10 °C to afford compound **7** as a red crystalline solid. Yield: 71% (0.39 g). Anal. Calcd for C₂₀H₃₄Br₂NNiOP: C, 43.36; H, 6.19; N, 2.53. Found: C, 43.09; H, 6.28; N, 2.51. IR (Nujol mull): v(C═N) 1596 cm^{-1}. ^{1}H NMR (25 °C, CD₂Cl₂, 300 MHz): δ 1.14 (d, 6H, $^3J_{HH}$ = 7 Hz, aryl-CH*Me*Me), 1.51 (d, 6H, $^3J_{HH}$ = 7 Hz, aryl-CHMe*Me*), 1.62 (bs, 6H, PCH*Me*Me), 1.75 (bs, 6H, PCHMe*Me*), 1.79 (s, 3H, *Me*C(O)N), 2.70 (m, 2H, PCHMe₂), 3.27 (hept, 2H, $^3J_{HH}$ = 7 Hz, aryl-CHMe₂), 7.13 (d, 2H, $^3J_{HH}$ = 7 Hz, m-CH$_{ar}$), 7.24 (t, 1H, $^3J_{HH}$ = 7 Hz, p-CH$_{ar}$). ^{13}C{^{1}H} NMR (25 °C, CD₂Cl₂, 75 MHz): δ 16.6 (s, PCH*Me*Me), 17.7 (s, *Me*C(O)N), 18.5 (s, PCHMe*Me*), 23.5 (s, aryl-CH*Me*Me), 23.8 (s, aryl-CHMe*Me*), 29.4 (s, aryl-CHMe₂), 29.8 (s, PCHMe₂), 123.9 (s, m-CH$_{ar}$), 128.1 (s, p-CH$_{ar}$), 140.6 (s, N-C$_{ar}$), 141.6 (s, o-C$_{ar}$),

173.7 (s, *Me*C(O)N). ³¹P{¹H} NMR (25 °C, CD₂Cl₂, 121 MHz): δ 178.0 (bs).

Synthesis of Ni[N-(2,6-iPr₂C₆H₃)=C((CH₃)₃OPiPr₂)]Br₂ **(8)**. A THF solution of ligand **3** (0.5 mmol) prepared in situ as described above was added at −78 °C to 154 mg of NiBr₂(dme) (0.5 mmol) suspended in 10 mL of THF. The reaction mixture was stirred and allowed to warm to room temperature over 30 min. The solvent was evaporated under reduced pressure, affording a red solid that was extracted with 40 mL of CH₂Cl₂. The solution was taken to dryness, and the residue was washed with 3 × 20 mL of hot diethyl ether (to remove any N-arylacetamide remaining in the mixture) and recrystallized from a mixture of CH₂Cl₂/toluene (2:1) at −10 °C to yield compound **8** as a red crystalline solid. Yield: 89% (0.26 g). Anal. Calcd for C₂₃H₄₀Br₂NNiOP: C, 46.35; H, 6.76; N, 2.35. Found: C, 46.85; H, 6.98; N, 2.27. IR (Nujol mull): ν(C=N) 1646 cm⁻¹. ¹H NMR (25 °C, CD₂Cl₂, 300 MHz): δ 1.09 (s, 9H, *tBu*C(O)N), 1.30 (d, 6H, ³*J*ₕₕ = 7 Hz, aryl-CH*Me*Me), 1.63 (bs, 6H, PCH*Me*Me), 1.73 (d, 6H, ³*J*ₕₕ = 7 Hz, aryl-CHMe*Me*), 1.75 (bs, 6H, PCHMe*Me*), 2.68 (m, 2H, PC*H*Me₂), 3.23 (h, 2H, ³*J*ₕₕ = 7 Hz, aryl-C*H*Me₂), 7.04 (d, 2H, ³*J*ₕₕ = 8 Hz, *m*-CHₐᵣ), 7.19 (t, 1H, ³*J*ₕₕ = 7 Hz, *p*-CHₐᵣ). ¹³C{¹H} NMR (25 °C, CD₂Cl₂, 75 MHz): δ 16.8 (s, PCH*Me*Me), 18.7 (s, PCHMe*Me*), 23.4 (s, aryl-CH*Me*Me), 24.5 (s, aryl-CHMe*Me*), 29.2 (s, *Me*₃CC(O)N), 29.3 (s, aryl-CHMe₂), 30.1 (s, PCHMe₂), 41.6 (s, Me₃*C*C(O)N), 123.3 (s, *m*-CHₐᵣ), 128.4 (s, *p*-CHₐᵣ), 140.5 (s, N-Cₐᵣ), 141.5 (s, *o*-Cₐᵣ), 177.5 (s, *t*BuC(O)N). ³¹P{¹H} NMR (25 °C, CD₂Cl₂, 121 MHz): δ 166.6 (bs).

Synthesis of Ni[N-(2,6-iPr₂C₆H₃)=C((CH₃)OPtBu₂)]Br₂ **(9)**. A 2 mL (1 mmol) portion of a 0.5 M THF solution of ligand **5** was added to a suspension of NiBr₂(dme) (308 mg, 1 mmol) in 10 mL of THF cooled to −60 °C. The reaction mixture was allowed to warm to room temperature while stirring. After 30 min, the solvent was removed under vacuum, and the red solid thus obtained was extracted with 60 mL of CH₂Cl₂ and filtered. The solution was then taken to dryness. The residue was washed with 2 × 20 mL of hexane and recrystallized from a mixture CH₂Cl₂/toluene (2:1) at −10 °C to afford compound **9** as a red crystalline solid. Yield: 72% (0.42 g). Anal. Calcd for C₂₂H₃₈Br₂NNiOP: C, 45.50; H, 6.58; N, 2.41. Found: C, 45.62; H, 6.44; N, 2.36. IR (Nujol mull): ν(C=N) 1606 cm⁻¹. ¹H NMR (25 °C, CD₂Cl₂, 300 MHz): δ 1.14 (d, 6H, ³*J*ₕₕ = 7 Hz, aryl-CH*Me*Me), 1.51 (d, 6H, ³*J*ₕₕ = 7 Hz, aryl-CHMe*Me*), 1.78 (bs, 18H, PCMe₃), 1.80 (s, 3H, *Me*C(O)N), 3.23 (m, 2H, aryl-C*H*Me₂), 7.12 (d, 2H, ³*J*ₕₕ = 8 Hz, *m*-CHₐᵣ), 7.23 (t, 1H, ³*J*ₕₕ = 8 Hz, *p*-CHₐᵣ). ¹³C{¹H} NMR (25 °C, CD₂Cl₂, 75 MHz): δ 18.1 (s, *Me*C(O)N), 23.6 (s, aryl-CH*Me*Me), 23.9 (s, aryl-CHMe*Me*), 28.9 (s, PCMe₃), 29.4 (s, aryl-CHMe₂), 42.7 (s, PCMe₃), 123.9 (s, *m*-CHₐᵣ), 128.1 (s, *p*-CHₐᵣ), 140.9 (s, N-Cₐᵣ), 141.8 (s, *o*-Cₐᵣ), 173.6 (s, *Me*C(O)N). ³¹P{¹H} NMR (25 °C, CD₂Cl₂, 121 MHz): δ 198.0 (bs).

Synthesis of Pd[N-(2,6-iPr₂C₆H₃)=C((CH₃)OPiPr₂)]Cl₂ **(10)**. A 20 mL portion of a THF solution of ligand **1** (1 mmol) prepared in situ as described above was added at −78 °C to a suspension of PdCl₂(cod) (285 mg, 1 mmol) in 10 mL of THF. The reaction mixture was stirred while being allowed to warm to room temperature over 1 h. The solvent was evaporated under vacuum, and the residue was extracted with 50 mL of CH₂Cl₂. The solution was then taken to dryness, affording a yellow solid that was recrystallized from THF at −10 °C to yield compound **10**. Yield: 96% (0.56 g). Anal. Calcd for C₂₀H₃₄Cl₂NOPPd: C, 46.48; H, 6.68; N, 2.73. Found: C, 46.36; H, 6.57; N, 2.86. IR (Nujol mull): ν(C=N) 1604 cm⁻¹. ¹H NMR (25 °C, CD₂Cl₂, 300 MHz): δ 1.15 (d, 6H, ³*J*ₕₕ = 7 Hz, aryl-CH*Me*Me), 1.40 (d, 6H, ³*J*ₕₕ = 7 Hz, aryl-CHMe*Me*), 1.43 (dd, 6H, ³*J*ₕₕ = 7 Hz, ³*J*ₕₚ = 20 Hz, PCH*Me*Me), 1.60 (dd, 6H, ³*J*ₕₕ = 7 Hz, ³*J*ₕₚ = 14 Hz, PCHMe*Me*), 1.97 (s, 3H, *Me*C(O)N), 2.71 (d hept, 2H, ³*J*ₕₕ = 7 Hz, ²*J*ₕₚ = 14 Hz, PC*H*Me₂), 2.99 (hept, 2H, ³*J*ₕₕ = 7 Hz, aryl-C*H*Me₂), 7.20 (d, 2H, ³*J*ₕₕ = 8 Hz, *m*-CHₐᵣ), 7.32 (t, 1H, ³*J*ₕₕ = 8 Hz, *p*-CHₐᵣ). ¹³C{¹H} NMR (25 °C, CD₂Cl₂, 75 MHz): δ 16.4 (d, ²*J*ᴄₚ = 3 Hz, PCH*Me*Me), 17.2 (s, *Me*C(O)N), 17.2 (d, ²*J*ᴄₚ = 1 Hz, PCHMe*Me*), 23.4 (s, aryl-CH*Me*Me), 23.6 (s, aryl-CHMe*Me*), 29.2 (s, aryl-CHMe₂), 30.0 (d, ¹*J*ᴄₚ = 24 Hz, PCHMe₂), 124.0 (s, *m*-CHₐᵣ), 128.6 (s, *p*-CHₐᵣ), 139.3 (s, N-Cₐᵣ), 141.7 (s, *o*-Cₐᵣ), 174.2 (s, *Me*C(O)N). ³¹P{¹H} NMR (25 °C, CD₂Cl₂, 121 MHz): δ 201.5 (s).

Synthesis of Pd[N-(2,6-iPr₂C₆H₃)=C(C(CH₃)₃OPiPr₂)]Cl₂ **(11)**. A THF solution of ligand **3** (0.5 mmol) prepared in situ as described above was added at −78 °C to 143 mg of PdCl₂(cod) (0.5 mmol) suspended in 10 mL of THF. The reaction mixture was stirred and allowed to warm to room temperature over 30 min. The solvent was evaporated under reduced pressure, affording a yellow solid that was extracted with 30 mL of CH₂Cl₂. The solution was taken to dryness, and the residue was recrystallized from THF at −10 °C to yield compound **11** as a yellow crystalline solid. Yield: 97% (0.27 g). Anal. Calcd for C₂₃H₄₀Cl₂NOPPd: C, 49.79; H, 7.27; N, 2.52. Found: C, 49.63; H, 7.31; N, 2.58. IR (Nujol mull): ν(C=N) 1647 cm⁻¹. ¹H NMR (25 °C, CD₂Cl₂, 300 MHz): δ 1.11 (s, 9H, *tBu*C(O)N), 1.31 (d, 6H, ³*J*ₕₕ = 7 Hz, aryl-CH*Me*Me), 1.51 (dd, 6H, ³*J*ₕₕ = 7 Hz, ³*J*ₕₚ = 20 Hz, PCH*Me*Me), 1.52 (d, 6H, ³*J*ₕₕ = 7 Hz, aryl-CHMe*Me*), 1.61 (dd, 6H, ³*J*ₕₕ = 7 Hz, ³*J*ₕₚ = 20 Hz, PCHMe*Me*), 2.71 (m, 2H, PC*H*Me₂), 2.97 (h, 2H, ³*J*ₕₕ = 8 Hz, aryl-C*H*Me₂), 7.10 (d, 2H, ³*J*ₕₕ = 8 Hz, *m*-CHₐᵣ), 7.24 (t, 1H, ³*J*ₕₕ = 7 Hz, *p*-CHₐᵣ). ¹³C{¹H} NMR (25 °C, CD₂Cl₂, 75 MHz): δ 16.3 (d, ²*J*ᴄₚ = 2 Hz, PCH*Me*Me), 17.3 (d, ²*J*ᴄₚ = 3 Hz, PCHMe*Me*), 23.3 (s, aryl-CH*Me*Me), 24.1 (s, aryl-CHMe*Me*), 29.1 (s, aryl-CHMe₂), 29.3 (s, *Me*₃CC(O)N), 30.2 (d, ¹*J*ᴄₚ = 26 Hz, PCHMe₂), 41.9 (d, ¹*J*ᴄₚ = 4 Hz, Me₃*C*C(O)N), 123.4 (s, *m*-CHₐᵣ), 128.2 (s, *p*-CHₐᵣ), 139.6 (s, N-Cₐᵣ), 141.2 (s, *o*-Cₐᵣ), 177.8 (s, *t*BuC(O)N). ³¹P{¹H} NMR (25 °C, CD₂Cl₂, 121 MHz): δ 194.5 (s).

Synthesis of Pd[N-(2,6-iPr₂C₆H₃)=C((CH₃)OPtBu₂)]Cl₂ **(12)**. A 0.9 mL (0.5 mmol) portion of a 0.5 M THF solution of ligand **5** was added to 143 mg of PdCl₂(cod) (0.5 mmol) suspended in 20 mL of THF. After stirring for 30 min, the solvent was removed under vacuum. The yellow solid thus obtained was washed with 2 × 10 mL of hexane and recrystallized from THF to afford compound **12** as a yellow crystalline solid. Yield: 91% (0.25 g). Anal. Calcd for C₂₂H₃₈Cl₂NOPPd: C, 48.86; H, 7.08; N, 2.59. Found: C, 48.81; H, 6.74; N, 2.67. IR (Nujol mull): ν(C=N) 1611 cm⁻¹. ¹H NMR (25 °C, CD₂Cl₂, 300 MHz): δ 1.15 (d, 6H, ³*J*ₕₕ = 7 Hz, aryl-CH*Me*Me), 1.38 (d, 6H, ³*J*ₕₕ = 7 Hz, aryl-CHMe*Me*), 1.64 (d, 18H, ³*J*ₕₚ = 16 Hz, PC*Me*₃), 1.99 (s, 3H, *Me*C(O)N), 2.99 (m, 2H, aryl-C*H*Me₂), 7.19 (d, 2H, ³*J*ₕₕ = 8 Hz, *m*-CHₐᵣ), 7.31 (t, 1H, ³*J*ₕₕ = 8 Hz, *p*-CHₐᵣ). ¹³C{¹H} NMR (25 °C, CD₂Cl₂, 75 MHz): δ 17.2 (d, ³*J*ᴄₚ = 4 Hz, *Me*C(O)N), 23.5 (s, aryl-CH*Me*Me), 23.6 (s, aryl-CHMe*Me*), 27.7 (d, ²*J*ᴄₚ = 4 Hz, PC*Me*₃), 29.1 (s, aryl-CHMe₂), 42.5 (d, ¹*J*ᴄₚ = 12 Hz, PCMe₃), 124.0 (s, *m*-CHₐᵣ), 128.5 (s, *p*-CHₐᵣ), 139.6 (s, N-Cₐᵣ), 141.8 (s, *o*-Cₐᵣ), 174.2 (s, *Me*C(O)N). ³¹P{¹H} NMR (25 °C, CD₂Cl₂, 121 MHz): δ 206.8 (s).

Computational Details. *Geometry Optimizations.* Guess structures for the square-planar (S = 0) and tetrahedral (S = 1) structures of complex **7** were obtained with the semiempirical PM3 method implemented in the Spartan 08 software.[62] The structures were subjected to full optimization with DFT methods with the Gaussian package.[63] Two series of calculations were carried out using the B3LYP or BP86 functionals. In either case, the metal atom and all atoms directly bound were described with the 6-311G* basis set, and the 6-31G* basis was used for the rest. Geometry minima were checked with frequency calculations.

NMR Spectral Simulation. Spectral simulations of the variable-temperature ¹H NMR spectra of **7** were carried out with the gNMR program.[64] Full line-shape analysis was assisted by a least-squares optimization of the simulated and experimental spectra. The fluxional process was modeled as an exchange between the diamagnetic complex, containing the spin system observed in the slow limit, and the paramagnetic species, which was described as two independent spin systems, one of them containing the P atom and the other, the H atoms, in order to ensure complete loss of coupling information. Even though the parameters for the paramagnetic species are unknown, for the purpose of the simulation, their precise values are not important and proof values were used to describe a very small equilibrium concentration and very large chemical shifts typical of such substances. The fact that the thermal drift of the average resonances changes very little over the studied temperature range confirms that the concentration of the paramagnetic species is small. In this case, the exchange rate equals the product *k*[SP], where *k* is the rate constant (square-planar to tetrahedral) and [SP] is the concentration of the

Table 5. Summary of Crystallographic Data and Structure Refinement Results for 7−12

compound	7	8	9	10	11	12·0.5THF
chemical formula	$C_{20}H_{34}Br_2NNiOP$	$C_{23}H_{40}Br_2NNiOP$	$C_{22}H_{38}Br_2NNiOP$	$C_{20}H_{34}Cl_2NOPPd$	$C_{23}H_{40}Cl_2NOPPd$	$C_{22}H_{38}Cl_2NOPPd\cdot0.5(C_4H_8O)$
formula mass	553.98	596.06	582.03	512.75	554.83	1153.71
cryst syst	monoclinic	orthorhombic	monoclinic	monoclinic	orthorhombic	triclinic
a/Å	10.7905(7)	15.7309(13)	11.2189(9)	10.884(2)	17.5777(5)	9.8987(14)
b/Å	14.5510(9)	11.6766(7)	14.3721(12)	14.625(3)	10.4053(3)	14.667(2)
c/Å	15.0980(9)	14.6596(10)	15.8988(11)	17.988(4)	14.3919(4)	20.625(3)
α/deg	90.00	90.00	90.00	90.00	90.00	69.682(4)
β/deg	94.0900(10)	90.00	95.171(2)	122.881(3)	90.00	88.388(5)
γ/deg	90.00	90.00	90.00	90.00	90.00	77.260(4)
unit cell volume/Å^3	2364.5(3)	2692.7(3)	2553.1(3)	2404.5(8)	2632.30(13)	2735.1(7)
temp/K	100(2)	173(2)	173(2)	298(2)	100(2)	100(2)
space group	$P2_1/n$	$Pna2_1$	$P2_1/n$	$P2_1/c$	$Pna2_1$	$P\bar{1}$
no. of formula units per unit cell, Z	4	4	4	4	4	2
radiation type	Mo Kα	Mo Kα	Mo Kα	Mo Kα	Mo Kα	Mo Kα
absorption coefficient, μ/mm^{-1}	4.277	3.761	3.965	1.070	0.983	0.950
no. of reflns measured	15298	30958	49005	20505	19357	42159
no. of independent reflns	5987	4231	7573	4160	7174	16583
R_{int}	0.0289	0.0600	0.0445	0.0275	0.0173	0.0270
final $R_1{}^a$ values $[F^2 > 2\sigma(F^2)]$	0.0347	0.0562	0.0636	0.0231	0.0145	0.0253
final $wR(F^2)^b$ values $[F^2 > 2\sigma(F^2)]$	0.0901	0.1420	0.1607	0.0615	0.0368	0.0673
final $R_1{}^a$ values (all data)	0.0476	0.0692	0.0755	0.0266	0.0154	0.0319
final $wR(F^2)^b$ values (all data)	0.0931	0.1503	0.1725	0.0628	0.0373	0.0692
goodness of fit on F^2, S^c	0.987	1.144	1.061	1.042	1.045	1.080

$^a R_1(F) = \sum(|F_o| - |F_c|)/\sum|F_o|$. $^b wR_2(F^2) = \{\sum[w(F_o{}^2 - F_c{}^2)^2]/\sum w(F_o{}^2)^2\}^{1/2}$. $^c S = \{\sum[w(F_o{}^2 - F_c{}^2)^2]/(n - p)\}^{1/2}$ (n = number of reflections, p = number of parameters).

square-planar species, which can be approximated to the total concentration of the complex. It was independently checked that different proof values of the paramagnetic chemical shifts had no significant effect on the spectral line shape, provided that these are very large in comparison with the normal diamagnetic shifts of the diamagnetic compound. For a final refinement of the simulation, the equilibrium constant was estimated from the free activation energy, which is not far from the energy difference between the square-planar and the tetrahedral species.

Ethylene Oligomerization Reactions: General Procedure. These reactions were carried out in 250 mL Fischer-Porter glass reactors provided with a septum-capped injection port, an internal thermocouple probe, and magnetic stirring. The reactor was previously oven-dried. It was then degassed in the vacuum line and charged with the prescribed amounts of solvent (toluene) and catalyst, the latter as a standard solution in CH_2Cl_2 (4.5×10^{-3} or 2.25×10^{-4} M). It was then immersed in a thermostat water bath and connected to the ethylene line. After purging three times with ethylene to remove the original N_2 atmosphere, the device was allowed to equilibrate at the required temperature and pressure. At this point, a cocatalyst solution (MMAO 1.9 M in heptane, Akzo-Nobel, or DEAC 0.25 M in toluene) was added. A color change from purple to yellow can be noticed. Ethylene was continuously fed into the reactor from a external reservoir with a calibrated volume to maintain a constant pressure in the reactor. The pressure drop in the reservoir was used to monitor the monomer consumption. The experiments were terminated by releasing the pressure and pouring the mixture in a beaker. These were stored in closed containers at −20 °C until GC analyses were performed. Quantitative GC analyses were made using the CH_2Cl_2 peak as an internal standard. The reaction mixtures were only slightly hazy and, upon treatment with acidified methanol, did not produce any significant precipitate of polyethylene. Key experiments were repeated to ensure the reproducibility of the data, which was found to be within 10−15%.

X-ray Structure Analysis for 7, 8, 9, 10, 11, and 12·THF. A summary of crystallographic data and structure refinement results for these new crystalline compounds are given in Table 5. Crystals coated with dry perfluoropolyether were mounted on glass fibers and fixed in a cold nitrogen stream. Intensity data were collected on a Bruker-AXS Apex CCD diffractometer (**7** and **10**) or on a Bruker-Nonius X8Kappa Apex II CCD diffractometer (**8, 9, 11,** and **12·0.5THF**), operating both with graphite monochromated Mo Kα radiation ($\lambda = 0.71073$ Å). The data were reduced by SAINT[65] and corrected for absorption effects by the multiscan method (SADABS).[65] The structures were solved by direct methods (SIR-2002, SHELXS)[66,67] and refined against all F^2 data by full-matrix least-squares techniques (SHELXTL-6.12)[65] minimizing $w[F_o{}^2 - F_c{}^2]^2$. All non-hydrogen atoms were refined with anisotropic thermal parameters. Hydrogen atoms were included in calculated positions and allowed to ride on the attached carbon atoms with the isotropic temperature factors (U_{iso} values) fixed at 1.2 times those U_{eq} values of the corresponding carbon atoms (1.5 times for the methyl groups).

■ ASSOCIATED CONTENT

Ⓢ Supporting Information

CIF file containing crystallographic data for complexes **7−11** and **12·0.5THF**. This material is available free of charge via the Internet at http://pubs.acs.org.

■ AUTHOR INFORMATION

Corresponding Author

*E-mail: campora@iiq.csic.es.

■ ACKNOWLEDGMENTS

■ REFERENCES

(1) (a) Braunstein, P. *Chem. Rev.* **2006**, *106*, 134. (b) Braunstein, P.; Naud, F. *Angew. Chem., Int. Ed.* **2001**, *40*, 680.

(2) (a) Nakamura, A.; Ito, S.; Nozaki, K. *Chem. Rev.* **2009**, *109*, 215. (b) Berkfield, A.; Mecking, S. *Angew. Chem., Int. Ed.* **2008**, *47*, 2538.

(3) (a) Liang, L.-C. *Coord. Chem. Rev.* **2006**, *250*, 1152. (b) Maggini, S. *Coord. Chem. Rev.* **2009**, *253*, 1793. (c) van der Vlugt, J. I.; Reek, J. N. H. *Angew. Chem., Int. Ed.* **2009**, *48*, 8832.

(4) Helmchen, G.; Pfaltz, A. *Acc. Chem. Res.* **2000**, *33*, 336.

(5) McManus, H. A.; Guiry, P. J. *Chem. Rev.* **2004**, *104*, 4151.

(6) Guironnet, D.; Caporaso, L.; Neuwald, B.; Göttker-Schnetmann, I.; Cavallo, L.; Mecking, S. *J. Am. Chem. Soc.* **2010**, *132*, 4418.

(7) (a) Haras, A.; Michalak, A.; Rieger, B.; Ziegler, T. *J. Am. Chem. Soc.* **2008**, *127*, 8765. (b) Noda, S.; Nakamura, A.; Kochi, T.; Chung, L. W.; Morokuma, K.; Nozaki, K. *J. Am. Chem. Soc.* **2009**, *121*, 14088.

(8) Speiser, F.; Braunstein, P.; Saussine, L. *Acc. Chem. Res.* **2005**, *38*, 784.

(9) Younkin, T. R.; Connor, E. F.; Henderson, J. I.; Friedrich, S. K.; Grubbs, R. H.; Bansleben, D. A. *Science* **2000**, *287*, 460.

(10) Kermagoret, A.; Braunstein, P. *Organometallics* **2008**, *27*, 88.

(11) Vogt, D. In *Applied Homogeneous Catalysis with Organometallic Compounds*; Cornils, B., Herrmann, W. A., Eds.; Wiley-VCH: Weinheim, Germany, 2002; Vol. 1, p 245.

(12) Ravasio, A.; Boggioni, L.; Tritto, I. In *Olefin Upgrading Catalysis by Nitrogen-based Metal Complexes*; Gianbastiani, G., Cámpora, J., Eds.; Springer: Dordrecht, The Netherlands, 2011.

(13) Skupinska, J. *Chem. Rev.* **1991**, *91*, 613.

(14) Keim, W. *Angew. Chem., Int. Ed.* **1990**, *29*, 235.

(15) Keim, W. *New J. Chem.* **1994**, 18.

(16) Kuhn, P.; Semeril, D.; Matt, D.; Chetcuti, M. J.; Lutz, P. *Dalton Trans.* **2007**, 515.

(17) Soula, R.; Broyer, J. P.; Llauro, M. F.; Tomov, A.; Spitz, R.; Claverie, J.; Drujon, X.; Malinge, J.; Saudemont, T. *Macromolecules* **2001**, *34*, 2438.

(18) Thapa, I.; Gambarotta, S.; Korobkov, I.; Duchateau, R.; Kulangara, S. V.; Chevalier, R. *Organometallics* **2010**, *29*, 4080.

(19) Forestière, A.; Olivier-Bourbigou, H.; Saussine, L. *Oil Gas Sci. Technol.* **2009**, *64*, 649.

(20) Guo, C.-Y.; Peulecke, N.; Basvani, K. R.; Kindermann, M. K.; Heinicke, J. *Macromolecules* **2010**, *43*, 1416.

(21) Chavez, P.; Rios, I. G.; Kermagoret, A.; Pattacini, R.; Meli, A.; Bianchini, C.; Giambastiani, G.; Braunstein, P. *Organometallics* **2009**, *28*, 1776.

(22) Flapper, J.; Kooijman, H.; Lutz, M.; Spek, A. L.; van Leeuwen, P.; Elsevier, C. J.; Kamer, P. C. J. *Organometallics* **2009**, *28*, 3272.

(23) Speiser, F.; Braunstein, P.; Saussine, L. *Organometallics* **2004**, *23*, 2625.

(24) Speiser, F.; Braunstein, P.; Saussine, L. *Organometallics* **2004**, *23*, 2633.

(25) Speiser, F.; Braunstein, P.; Saussine, L.; Welter, R. *Organometallics* **2004**, *23*, 2613.

(26) Speiser, F.; Braunstein, P.; Saussine, L.; Welter, R. *Inorg. Chem.* **2004**, *43*, 1649.

(27) Guan, Z.; Marshall, W. J. *Organometallics* **2002**, *21*, 3580.

(28) Chen, H.-P.; Liu, Y.-H.; Peng, S.-M.; Liu, S.-T. *Organometallics* **2003**, *22*, 4893.

(29) Daugulis, O.; Brookhart, M.; White, P. S. *Organometallics* **2002**, *21*, 5935.

(30) Flapper, J.; van Leeuwen, P. W. N. M.; Elsevier, C. J.; Kamer, P. C. J. *Organometallics* **2009**, *28*, 3264.

(31) van den Beuken, E. K.; Smeets, W. J. J.; Spek, A. L.; Feringa, B. L. *Chem. Commun.* **1998**, 223.

(32) Keim, W.; Killat, S.; Nobile, C. F.; Suranna, G. P.; Englert, U.; Wang, R.; Mecking, S.; Schröder, D. L. *J. Organomet. Chem.* **2002**, *662*, 150.

(33) Killian, C. M.; McDevitt, J. P.; Mackenzie, P. B.; Moody, L. S.; Ponasik, J. A., Jr. Patent WO 9840420, 1998.

(34) Buchard, A.; Auffrant, A.; Klemps, C.; Vu-Do, L.; Boubekeur, L.; Goff, X. F. L.; Floch, P. L. *Chem. Commun.* **2007**, 1502.

(35) Daugulis, O.; Brookhart, M. *Organometallics* **2002**, *21*, 5926.

(36) Johnson, L. K.; Killian, C. M.; Brookhart, M. *J. Am. Chem. Soc.* **1995**, *117*, 6414.

(37) Gates, D. P.; Svejda, S. A.; Oñate, E.; Killian, C. M.; Johnson, L. K.; White, P. S.; Brookhart, M. *Macromolecules* **2000**, *33*, 2320.

(38) Ittel, S. D.; Johnson, L. K.; Brookhart, M. *Chem. Rev.* **2000**, *100*, 1169.

(39) Tempel, D. J.; Johnson, L. K.; Huff, R. L.; White, P. S.; Brookhart, M. *J. Am. Chem. Soc.* **2000**, *122*, 6686.

(40) Guan, Z.; Popeney, C. S. In *Metal Catalysts in Olefin Polymerization*; Guan, Z., Ed.; Springer: Berlin, 2009.

(41) Speiser, F.; Braunstein, P.; Saussine, L. *Dalton Trans.* **2004**, 1539.

(42) Kühl, O. *Coord. Chem. Rev.* **2006**, *250*, 2867.

(43) Slawin, A. M. Z.; Wainwright, M.; Woollins, J. D. *J. Chem. Soc., Dalton Trans.* **2001**, 2724.

(44) Ly, T. Q.; Slawin, A. M. Z.; Woollins, J. D. *Angew. Chem., Int. Ed.* **1998**, *37*, 2501.

(45) Braunstein, P.; Frison, C.; Morise, X.; Adams, R. D. *J. Chem. Soc., Dalton Trans.* **2000**, 2205.

(46) Rodriguez i Zubiri, M.; Milton, H. L.; Slawin, A. M. Z.; Woollins, J. D. *Polyhedron* **2004**, *23*, 865.

(47) Bhattacharyya, P.; Ly, T. Q.; Slawin, A. M. Z.; Woollins, J. D. *Polyhedron* **2001**, *20*, 1803.

(48) Agostinho, M.; Rosa, V.; Aviles, T.; Welter, R.; Braunstein, P. *Dalton Trans.* **2009**, 814.

(49) Jones, N. G.; Green, M. L. H.; Vei, I.; Cowley, A.; Morise, X.; Braunstein, P. *J. Chem. Soc., Dalton Trans.* **2002**, 1487.

(50) Hosokawa, T. W. Y.; Hosokawa, K.; Tsuji, T.; Murahashi, S. I. *J. Chem. Soc., Chem. Commun.* **1996**, 859.

(51) Braunstein, P.; Heaton, B. T.; Jacob, C.; Manzi, L.; Morise, X. *Dalton Trans.* **2003**, 1396.

(52) Roucoux, A.; Thieffry, L.; Carpentier, J.-F.; Devocelle, M.; Meliet, C.; Agbossou, F.; Mortreux, A.; Welch, A. J. *Organometallics* **1996**, *15*, 2440.

(53) Harvey, J. N. *Annu. Rep. Prog. Chem., Sect. C* **2006**, *102*, 203.

(54) Svejda, S. A.; Johnson, L. K.; Brookhart, M. *J. Am. Chem. Soc.* **1999**, *121*, 10634.

(55) Tempel, D. J.; Johnson, L. K.; Huff, R. L.; White, P. S.; Brookhart, M. *J. Am. Chem. Soc.* **2000**, *122*, 6686.

(56) Shultz, L. H.; Tempel, D. J.; Brookhart, M. *J. Am. Chem. Soc.* **2001**, *123*, 11539.

(57) Leatherman, M. D.; Svejda, S. A.; Johnson, L. K.; Brookhart, M. *J. Am. Chem. Soc.* **2003**, *125*, 3068.

(58) Killian, C. M.; Johnson, L. K.; Brookhart, M. *Organometallics* **1997**, *16*, 2005.

(59) Ward, L. G. L.; Pipal, J. R. *Inorg. Synth.* **1971**, *13*, 154.

(60) Drew, D.; Doyle, J. R. *Inorg. Synth.* **1971**, *13*, 47.

(61) Boeré, R. T. K. V.; Wolmershäusser, G. *J. Chem. Soc., Dalton Trans.* **1998**, 4147.

(62) *Spartan 08*; Wavefunction, Inc.: Irvine, CA.

(63) Frisch, M. J.;et al. *Gaussian 03*, revision B.04; Gaussian, Inc.: Wallingford, CT, 2003.

(64) *gNMR 3.6 for Macintosh*; Cherwell Scientific Publishing Ltd.: Oxford, U.K.

(65) Bruker programs: *SMART*, version 5.629; *SAINT+*, version 6.45; *SADABS*, version 2.10; *SHELXTL*, version 6.12; Bruker AXS Inc.: Madison, WI, 2003.

(66) Burla, M. C.; Camalli, M.; Carrozzini, B.; Cascarano, G. L.; Giacovazzo, C.; Polidori, G.; Spagna, R. *J. Appl. Crystallogr.* **2003**, *36*, 1103.

(67) Sheldrick, G. M. *SHELX97: Program System for Crystal Structure Determination*; University of Göttingen: Göttingen, Germany, 1997.